ACS OMEGA

Open Access



http://pubs.acs.org/journal/acsodf

Article

# Transmembrane Prostate Androgen-Induced Protein 1 Molecular Modeling and Refinement Using Coarse-Grained Molecular Dynamics

Imam Adi Wicaksono, Wanda Destiarani, Shidqi Fajri Romadhon, Bagas Adi Prasetya Nugraha, Muhammad Yusuf, Tiana Milanda, and Riezki Amalia*

Cite This: *ACS Omega* 2025, 10, 2712−2724

Read Online

ACCESS | Metrics & More | Article Recommendations

**ABSTRACT:** Transmembrane prostate androgen-induced protein 1 (TMEPAI), a type 1b transmembrane protein, is highly expressed in many types of cancer and is involved in cancer signaling pathways. TMEPAI affects the TGF-$\beta$, androgen receptor, Wnt, and MAPK/ERK signaling pathways. Although TMEPAI interactions are known, information about their structure is limited. This study performed TMEPAI structure prediction via a computational approach with template-free modeling using multiple Web server and refining with coarse-grained molecular dynamics to improve the understanding of its characterization, mechanism, and interactions, followed by intensive server-based validation. As a result, the predicted TMEPAI isoform structure was validated for all parameters, and the trRosetta server provided the most reliable predicted structure. This research is expected to provide preliminary scientific information about the TMEPAI structure prediction and apply it to develop targeted cancer therapy drugs.

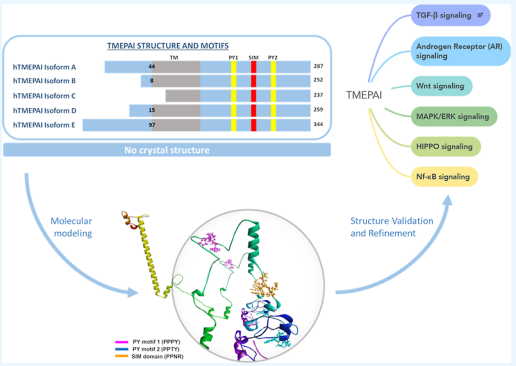


## INTRODUCTION

Transmembrane prostate androgen-induced protein 1 (TMEPAI), also known as prostate transmembrane protein androgen-induced 1 and solid tumor-associated gene 1, was initially identified as a prostate protein induced by testosterone or its derivatives.[1,2] TMEPAI is induced by TGF-$\beta$, mutant p53, MAPK/ERK, and Wnt,[1−5,] and it regulates androgen, TGF-$\beta$, Wnt HIPPO, NF-$\kappa$b, and JNK signaling.[6−13] TMEPAI is a type 1b transmembrane protein with five isoforms in humans, and it is composed of 237 to 344 amino acids with three main domains, consisting of an extracellular domain, transmembrane domain, and intracellular domain.[8,14] The protein−protein interactions of TMEPAI in the TGF-$\beta$ signaling pathway are SMAD2 and SMAD3,[5,8,9] and NEDD4L/NEDD4 is involved in the androgen receptor (AR) or EGF signaling pathway.[6,7,15]

TMEPAI is highly expressed in various cancers, such as breast, lung, and prostate cancers, and is associated with poor prognoses.[16] Genome-wide studies suggested that TMEPAI is one of the most highly inducible genes in invasive cancers, and it is known as a novel oncogenic protein.[17−19] Thus, this protein is a potential biomarker and target for anticancer therapy.[19,20]

To date, no solved TMEPAI structure has been reported, despite multiple studies about the molecular mechanism of TMEPAI. Thus, structure prediction with homology modeling is impractical for determination because of the lack of a highly similar protein. The structure of the closest protein homology, C18orf1, which has a protein sequence similarity to TMEPAI of 61%, also does not have a crystal structure.

Therefore, this research performed structural modeling prediction for TMEPAI isoforms through template-free modeling as an alternative approach to predicting the structures of TMEPAI isoforms and refining with coarse-grained molecular dynamics (CGMD). In this study, we investigated the predicted structures using three prediction servers with different modeling methods and subsequently validated the structure predictions.

## RESULTS AND DISCUSSION

Analysis of TMEPAI isoform sequence alignment and domain region. Analysis has been carried out to understand the structure, sequence alignment, and domain mapping of the TMEPAI isoforms in humans. Figure 1 reveals that TMEPAI

Received: September 14, 2024
Revised: December 20, 2024
Accepted: December 26, 2024
Published: January 14, 2025

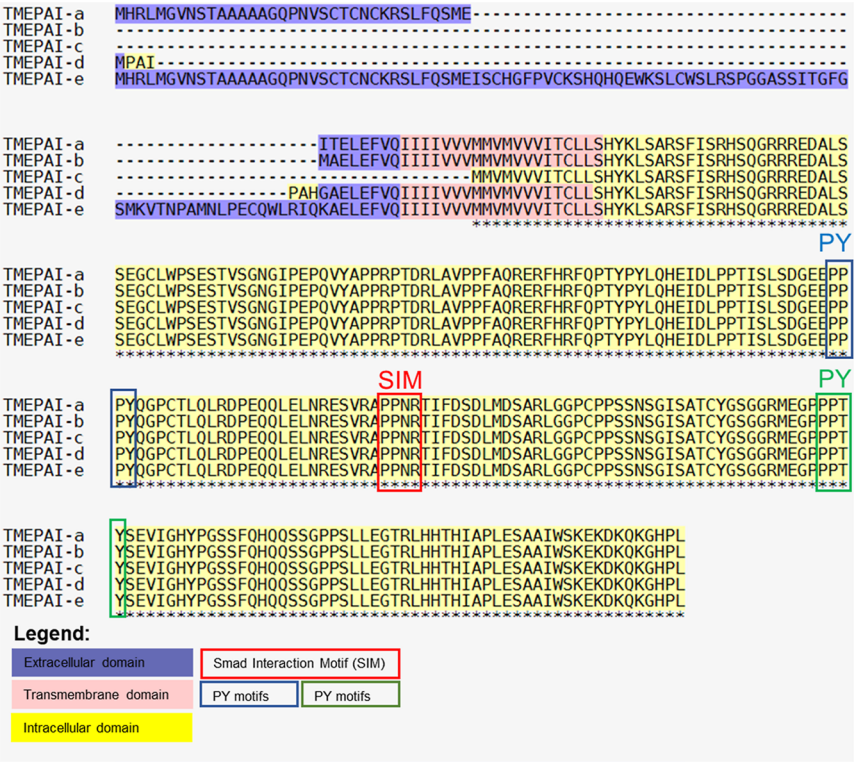


**Figure 1.** TMEPAI isoforms alignment and domain mapping were determined using the T-COFFEE multiple alignment server.

**Table 1. Physicochemical Parameters of TMEPAI Isoforms**

| parameters | TMEPAI-a | TMEPAI-b | TMEPAI-c | TMEPAI-d | TMEPAI-e |
|---|---|---|---|---|---|
| theoretical pI | 6.41 | 6.05 | 6.36 | 6.11 | 7.61 |
| negatively charged residues | 28 | 27 | 25 | 27 | 30 |
| positively charged residues | 25 | 22 | 22 | 22 | 31 |
| instability index | 68.99 | 65.86 | 69.23 | 65.89 | 68.31 |
| aliphatic index | 72.37 | 73.89 | 65.02 | 74.17 | 69.74 |
| GRAVY | −0.43 | −0.478 | −0.654 | −0.46 | −0.426 |

**Table 2. Amino Acid Composition of TMEPAI Isoforms**

| | TMEPAI-a | | TMEPAI-b | | TMEPAI-c | | TMEPAI-d | | TMEPAI-e | |
|---|---|---|---|---|---|---|---|---|---|---|
| amino acid | number | composition (%) | number | composition (%) | number | composition (%) | number | composition (%) | number | composition (%) |
| Ala | 16 | 5.6 | 12 | 4.8 | 11 | 4.6 | 14 | 5.4 | 19 | 5.5 |
| Arg | 19 | 6.6 | 17 | 6.7 | 17 | 7.2 | 17 | 6.6 | 21 | 6.1 |
| Asn | 7 | 2.4 | 4 | 1.6 | 4 | 1.7 | 4 | 1.5 | 9 | 2.6 |
| Asp | 9 | 3.1 | 9 | 3.6 | 9 | 3.8 | 9 | 3.5 | 9 | 2.6 |
| Cys | 8 | 2.8 | 5 | 2 | 5 | 2.1 | 5 | 1.9 | 12 | 3.5 |
| Gln | 16 | 5.6 | 14 | 5.6 | 13 | 5.5 | 14 | 5.4 | 20 | 5.8 |
| Glu | 19 | 6.6 | 18 | 7.1 | 16 | 6.8 | 18 | 6.9 | 21 | 6.1 |
| Gly | 20 | 7 | 18 | 7.1 | 18 | 7.6 | 19 | 7.3 | 25 | 7.3 |
| His | 11 | 3.8 | 10 | 4 | 10 | 4.2 | 11 | 4.2 | 14 | 4.1 |
| Ile | 15 | 5.2 | 14 | 5.6 | 10 | 4.2 | 15 | 5.8 | 17 | 4.9 |
| Leu | 23 | 8 | 21 | 8.3 | 20 | 8.4 | 21 | 8.1 | 27 | 7.8 |
| Lys | 6 | 2.1 | 5 | 2 | 5 | 2.1 | 5 | 1.9 | 10 | 2.9 |
| Met | 8 | 2.8 | 6 | 2.4 | 5 | 2.1 | 6 | 2.3 | 10 | 2.9 |
| Phe | 8 | 2.8 | 7 | 2.8 | 6 | 2.5 | 7 | 2.7 | 10 | 2.9 |
| Pro | 31 | 10.8 | 30 | 11.9 | 30 | 12.7 | 32 | 12.4 | 35 | 10.2 |
| Ser | 32 | 11.1 | 28 | 11.1 | 28 | 11.8 | 28 | 10.8 | 40 | 11.6 |
| Thr | 14 | 4.9 | 11 | 4.4 | 11 | 4.6 | 11 | 4.2 | 15 | 4.4 |
| Trp | 2 | 0.7 | 2 | 0.8 | 2 | 0.8 | 2 | 0.8 | 5 | 1.5 |
| Tyr | 8 | 2.8 | 8 | 3.2 | 8 | 3.4 | 8 | 3.1 | 8 | 2.3 |
| Val | 15 | 5.2 | 13 | 5.2 | 9 | 3.8 | 13 | 5 | 17 | 4.9 |



https://doi.org/10.1021/acsomega.4c08451
ACS Omega 2025, 10, 2712−2724

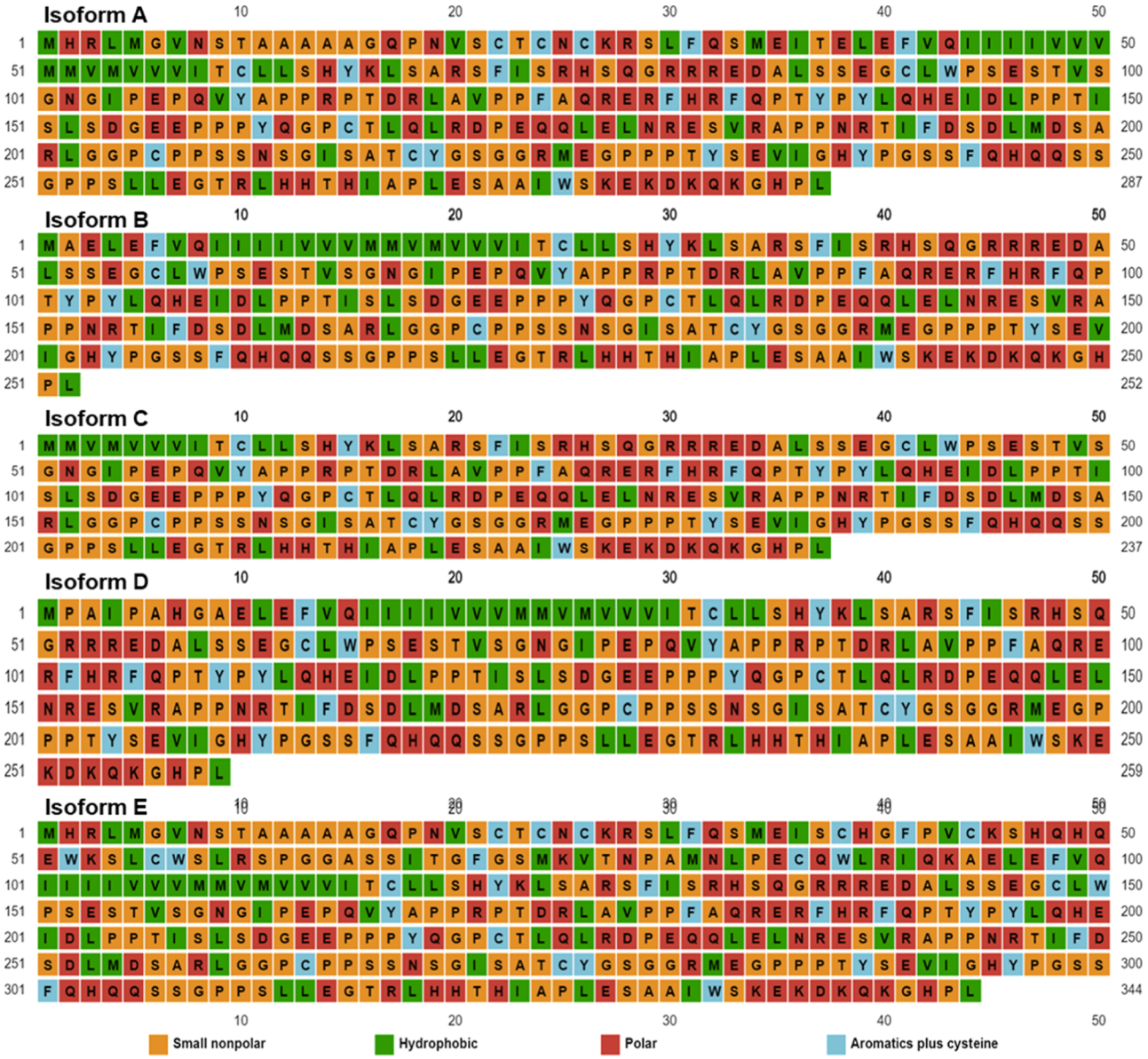


**Figure 2.** Amino acid composition of TMEPAI isoforms was determined using the PSIPRED server.

isoforms share two conserved PY motifs (blue and green boxes), a Smad interaction motif (SIM, red box), and a high-homology intracellular domain (yellow highlighting). TMEPAI exhibited variation in the extracellular and high-homology transmembrane domains, excluding TMEPAI-c, which only contained intracellular domains. TMEPAI is a type 1b transmembrane protein composed of three main domains: extracellular, transmembrane, and intracellular.[8] The cytoplasmic domain carries a PY (PPPY/PPTY) motif that can interact with the HECT E3 ubiquitin ligase NEDD4 and the PPNR motif involved in binding to the TGF-$\beta$–related protein Smad.[8,19,21,22] In humans, the TMEPAI protein has five known isoforms: a (287 amino acids), b (252 amino acids), c (237 amino acids), d (259 amino acids), and e (344 amino acids). TMEPAI-a, TMEPAI-b, and TMEPAI-c are the major isoforms expressed in prostate cancer cells and human prostate tumor tissue. TMEPAI-d and TMEPAI-e were characterized as minor isoforms with lower transcript levels. TMEPAI-a, TMEPAI-d, and TMEPAI-c transcripts have been detected in both AR-positive and AR-negative cancer cells.[14,20] The extracellular domains of the TMEPAI isoforms are diverse, suggesting structural differences. The intracellular domain is highly conserved, and the PY and SIM are present in TMEPAI isoforms in humans and mice. This conservation is essential to the function of TMEPAI in cancer signaling pathways and carcinogenesis.[8,19,21,22] Although laboratory experiments proved the function of TMEPAI in cancer, no specific study performed the structure prediction. This research performed structure prediction via template-free modeling and validation. Because of the lack of high-similarity proteins, the homology modeling prediction is unreliable.

**Analysis of Physicochemical Parameters.** The results for the physicochemical parameters of TMEPAI isoforms as determined using ExPASy's ProtParam Tool are presented in Table 1. The amino acid composition and types of TMEPAI isoforms are shown in Table 2 and Figure 2; small nonpolar amino acids (glycine and alanine) dominate all TMEPAI isoforms. The physicochemical parameters suggested that TMEPAI is an acidic protein. The isoelectric point of TMEPAI is 6.05–7.61, and it tends to be unstable (the instability index


https://doi.org/10.1021/acsomega.4c08451
ACS Omega 2025, 10, 2712−2724

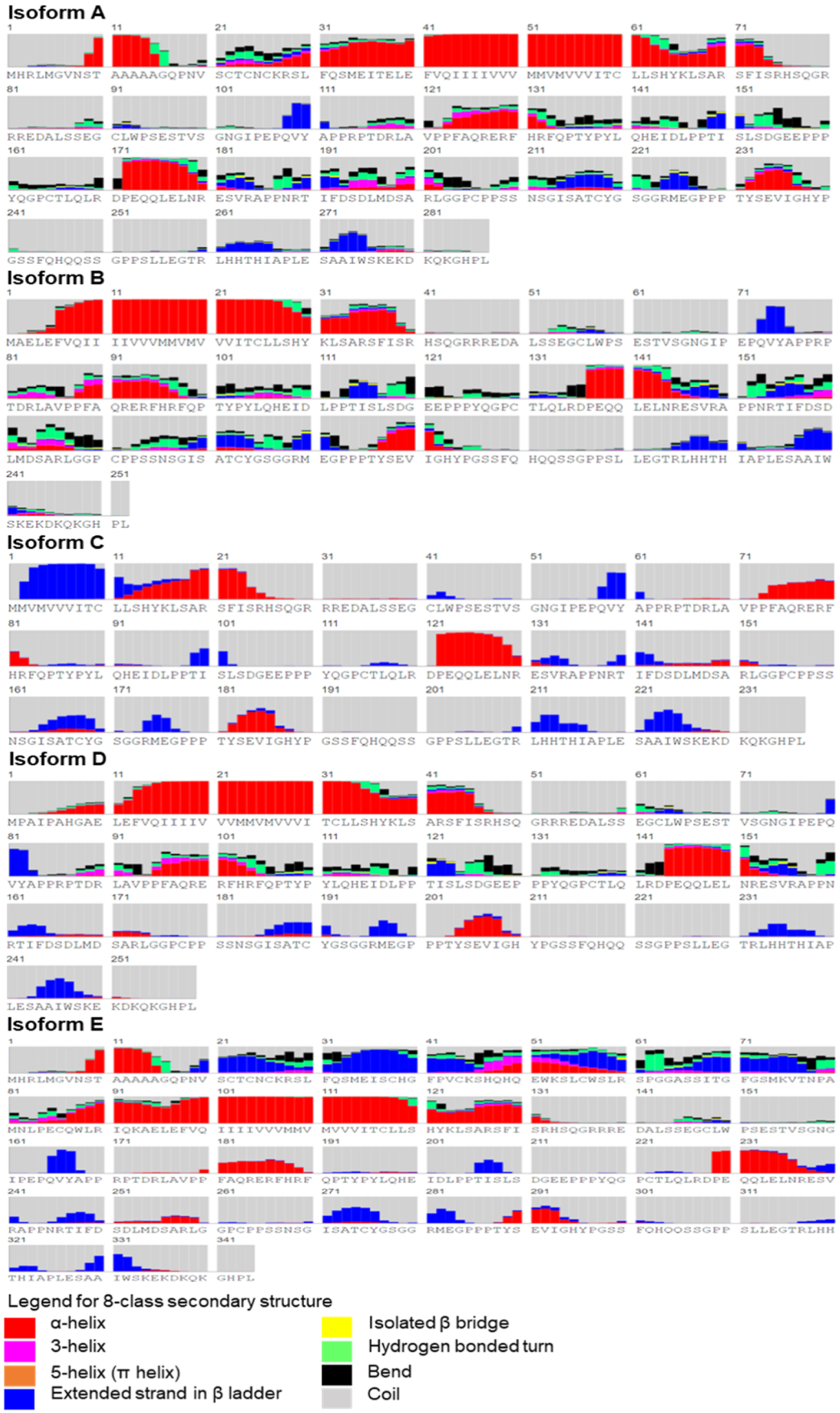


**Figure 3.** TMEPAI isoform secondary structure prediction using the RaptorX property.



https://doi.org/10.1021/acsomega.4c08451
*ACS Omega* 2025, 10, 2712−2724

>50) and thermostable globular protein (the aliphatic index >50). TMEPAI is a soluble protein because of the dominance of negatively charged residuals, and the protein more easily interacts with positively charged solvents or compounds. The average hydropathicity index for TMEPAI isoforms is negative (−0.43 to −0.654), indicating hydrophilicity. The amino acid composition revealed high serine (11% in TMEPAI-a and TMEPAI-e), proline content (12% in TMEPAI-b, TMEPAI-c, and TMEPAI-d), and low tryptophan content (0.7%−1.5% in TMEPAI isoforms).

TMEPAI secondary structure evaluation. The various parameters of the secondary structures were calculated by using the RaptorX and TMHMM 2.0 servers. Figure 3 presents the eight-class secondary structures of TMEPAI isoforms accessed using the RaptorX property server. The $\alpha$-helix was predicted to be located between amino acids 11−13 and 41−61 for isoform-a; amino acids 18−23 and 122−128 for isoform-b; amino acids 18−23 and 122−128 for isoform-c; amino acids 13−45 and 144−150 for isoform-d, and amino acids 9−14, 88−130, and 230−235 for isoform-e. The data revealed that the secondary structure dominantly consisted of coils (>70%), and more than 75% of the structure was exposed. Figure 4 presents the TMHMM 2.0 server prediction of the major regions of TMEPAI isoforms that generate the extracellular, transmembrane, and intracellular regions. TMEPAI-a, TMEPAI-b, TMEPAI-d, and TMEPAI-e all possessed these regions, whereas no transmembrane or intracellular region was identified for TMEPAI-c. RaptorX predicts the secondary structure using deep convolutional neural fields and conditional random fields. This server uses the area under the curve to predict proteins with irregular sequences.[23] The TMHMM 2.0 server predicts the helix/transmembrane structure using the hidden Markov model approach with 97−98% accuracy.[24] Secondary structure analysis revealed that TMEPAI-c lacks a transmembrane domain, making it an extracellular protein. A previous study suggested that TMEPAI-c is an intracellular protein with half of its sequence comprising a transmembrane domain.[8] This secondary structure analysis suggested that the predicted transmembrane regions of TMEPAI-a, TMEPAI-b, TMEPAI-d, and TMEPAI-e are hydrophobic.

Analysis of the TMEPAI isoform structure prediction. Analysis of the SWISS-MODEL template against the amino acid sequence library (STML) revealed that the sequence identity was less than 35% for the TMEPAI isoforms. TMEPAI-a had the highest sequence identity (10%, 40−64 amino acids) for SMTL ID 3s39.1 (PDB ID: 3S39; *Thermus thermophilus* cytochrome ba3 oxidase 60 s after Xe depressurization). TMEPAI-b had the highest sequence identity (13.79%, 7−35 amino acids) for SMTL ID 1ay2.1.a (PDB ID: 1AY2; fiber-forming protein pilin). TMEPAI-c had the highest sequence identity (32.14%, 41−62 amino acids) for SMTL ID 4oie.1.a (PDB ID: 4OIE, West Nile virus nonstructural protein NS1). TMEPAI-d and TMEPAI-e had the highest sequence identities of 14.29 (15−42 amino acids) and 13.33% (99−128 amino acids), respectively, for SMTL ID 3jc8.4 (PDB ID: 3JC8). The predicted structures generated by the trRosetta, RaptorX, Robetta, and AlphaFold servers are presented in Figure 5, and server assessment scores are shown in Table 3. The TMEPAI isoform structure prediction using the trRosetta server indicated that the TMEPAI-a, TMEPAI-b, TMEPAI-d, and TMEPAI-e structures have three domains, indicating a transmembrane structure. By contrast, TMEPAI-c has only two domains without a N-terminal domain (extracellular). All predicted structures had TM (transmembrane) scores within the trRosetta server assessment

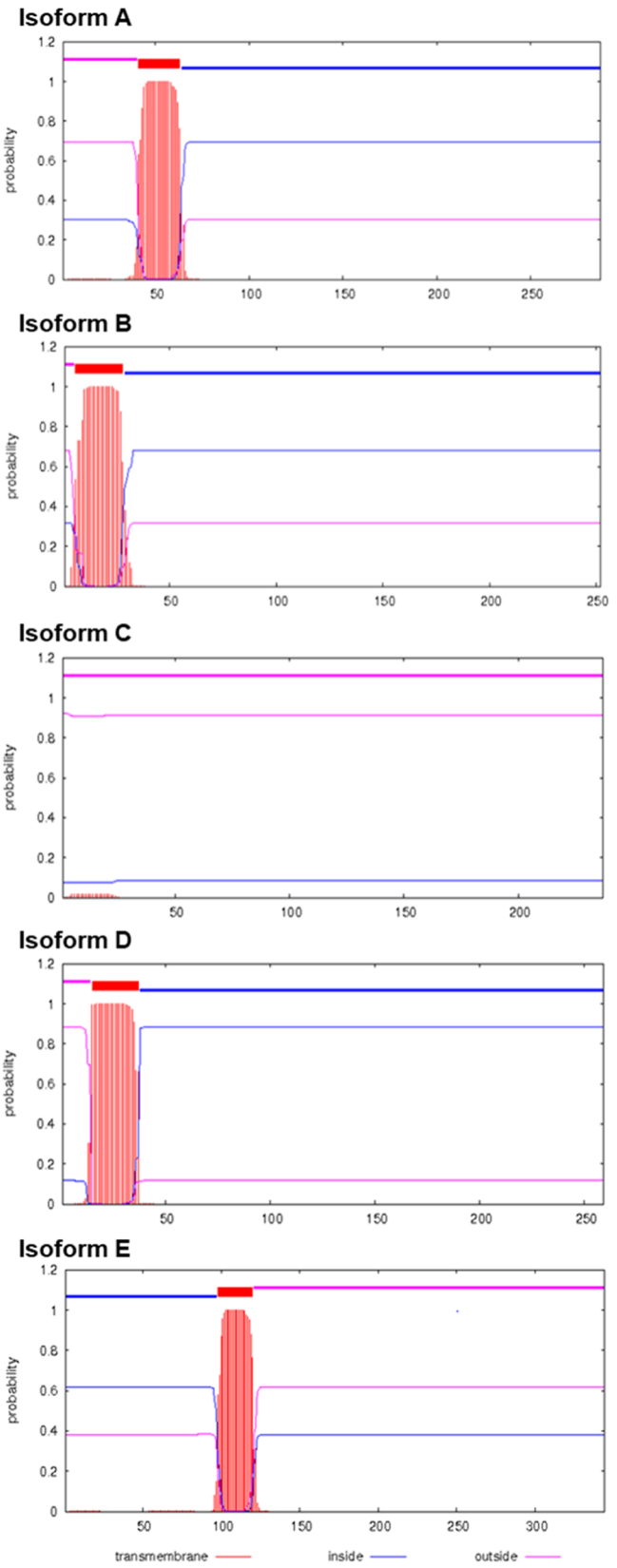


**Figure 4.** Transmembrane predictions for TMEPAI isoforms using the TMHMM 2.0 server.



https://doi.org/10.1021/acsomega.4c08451
*ACS Omega* 2025, 10, 2712−2724

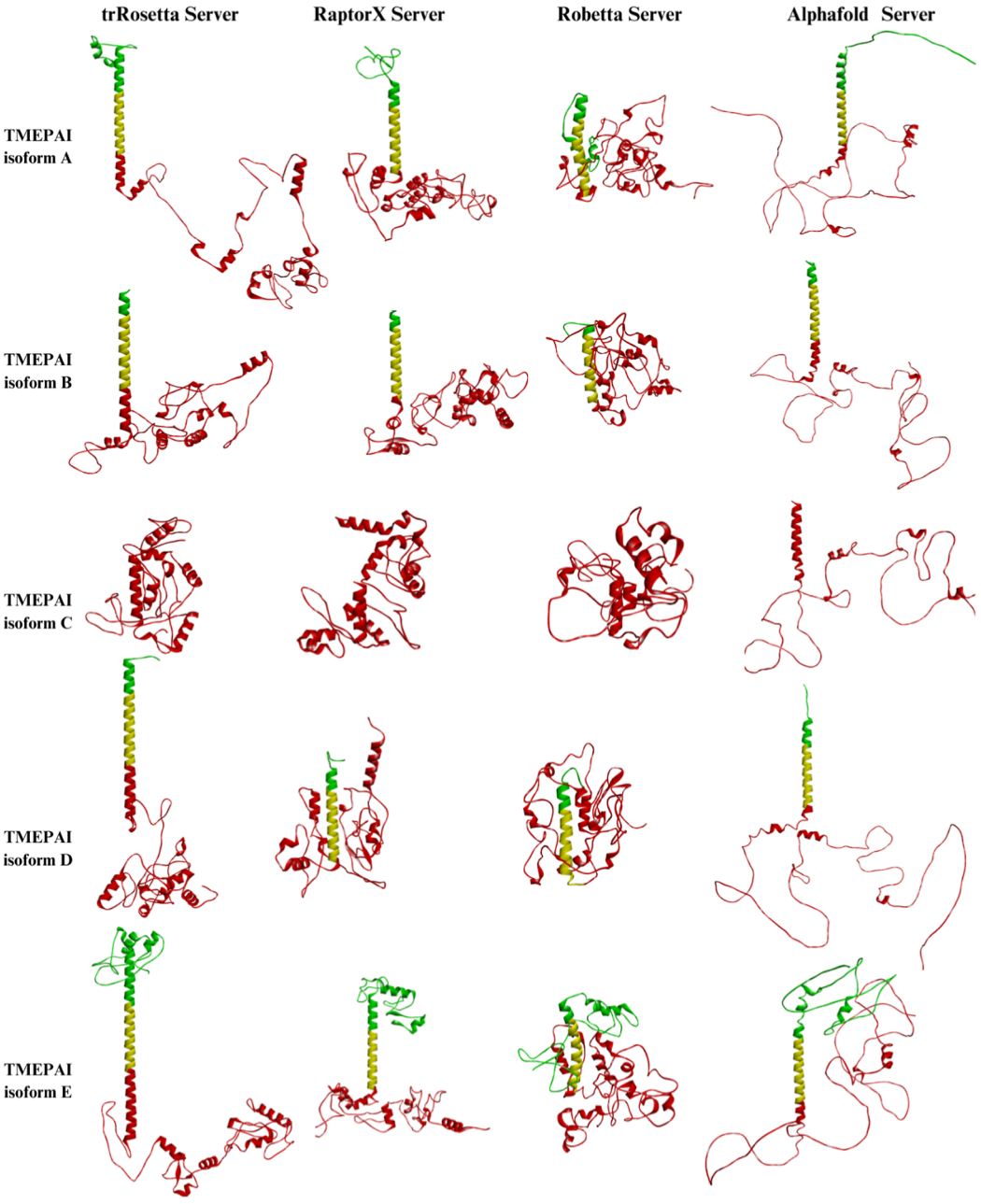


**Figure 5.** Models of the predicted structures of TMEPAI isoforms.

**Table 3. Model Server Assessment for the TMEPAI Isoform Structure Predictions**

| | protein modeling prediction servers | | | |
|---|---|---|---|---|
| TMEPAI isoform | trRosetta (TM-score = 0−1 Å) | raptorX (RMSD score <15 Å) | robetta (c-score = 0−1) | AlphaFold (pLDDT c-score = > 90) |
| TMEPAI-a | 0.208 Å | 11.280 Å | 0.14 | >90% only on $\alpha$-helix |
| TMEPAI-b | 0.203 Å | 10.552 Å | 0.15 | |
| TMEPAI-c | 0.192 Å | 10.316 Å | 0.13 | |
| TMEPAI-d | 0.208 Å | 13.021 Å | 0.16 | |
| TMEPAI-e | 0.214 Å | 10.825 Å | 0.13 | |

parameter. The TMEPAI isoform structure prediction using the RaptorX, Robetta, and AlphaFold servers revealed three domains for all isoforms, excluding TMEPAI-c. The RaptorX server assessment parameter obtained the root-mean-square deviation (RMSD) score results. The prediction model for all isoforms had a confidence score (c-score) as required by the Robetta server assessment parameter. AlphaFold produces a per-residue c-score (pLDDT) between 0 and 100. AlphaFold prediction model results had a very high c-score (>90%) only in the $\alpha$-helix structure (TM region). In comparison, most other regions had a very low c-score (<50%). Some regions with low pLDDT may be unstructured in isolation. The Rosetta server is currently regarded as the most successful template-free approach for CASP experiments.[25−27] For some



https://doi.org/10.1021/acsomega.4c08451
ACS Omega 2025, 10, 2712−2724

Table 4. Validation of the TMEPAI Prediction Servers

| TMEPAI isoform | protein modeling prediction servers | validation servers | | | |
|---|---|---|---|---|---|
| | | PROCHECK (≥90%)[a] | Verify3D (≥80%)[a] | QMEAN (Z-score ∼0)[a] | ERRAT (≥91%)[a] |
| TMEPAI-a | trRosetta | 91.5 | 26.48 | 1.11 | 85.8824 |
| | RaptorX | 83.3 | 64.81 | −1.71 | 83.1541 |
| | Robetta | 90.6 | 66.55 | −0.79 | 83.6957 |
| | AlphaFold | 49.1 | 10.45 | −14.28 | 68.478 |
| TMEPAI-b | trRosetta | 88.1 | 55.16 | 1.73 | 83.0918 |
| | RaptorX | 85.1 | 69.05 | −1.15 | 66.5272 |
| | Robetta | 90.6 | 65.87 | −0.65 | 88.5593 |
| | AlphaFold | 47.5 | 10.32 | −15.75 | 35.1145 |
| TMEPAI-c | trRosetta | 89.3 | 56.96 | 0.98 | 81.6514 |
| | RaptorX | 87.2 | 69.2 | 0.9 | 90.367 |
| | Robetta | 86.1 | 75.95 | −0.51 | 77.13 |
| | AlphaFold | 44.9 | 5.91 | −15.51 | 38.4348 |
| TMEPAI-d | trRosetta | 89.8 | 38.22 | 1.08 | 91.129 |
| | RaptorX | 82.5 | 73.75 | −1.1 | 80.4348 |
| | Robetta | 87.9 | 76.06 | 0.34 | 90.6504 |
| | AlphaFold | 45.1 | 4.25 | −17.00 | 32.4324 |
| TMEPAI-e | trRosetta | 87.9 | 54.07 | 0.92 | 79.6296 |
| | RaptorX | 84 | 59.01 | −1.80 | 71.6561 |
| | Robetta | 89.7 | 79.07 | 0.37 | 94.4615 |
| | AlphaFold | 30.9 | 2.62 | −21.96 | 12.621 |

[a]Server assessment parameter.

template-free targets, deep learning-based prediction of inter-residue orientations and distances and Rosetta's refinement of constrained optimization can create more accurate models.[28,29]

Validation of the TMEPAI isoform structure prediction. The validation result of the TMEPAI isoform structure prediction is presented in Table 4. The PROCHECK scores (most favored regions) ranged from 30.9 to 91.5%. The best quality criterion is a score exceeding 90%. Still, the structure quality is reliable if the most favored domain score is >80% and 0% amino acid residues are located in the disallowed regions. The quality and stability of the prediction are indicated by the presence of the majority of the amino acid residues in the most favored regions. The PROCHECK server verifies the quality of the predicted structure by analyzing the residue-by-residue geometry and overall structure geometry.[30] Verify3D determines the compatibility of an atomic model (in three dimensions) using the primary amino acid sequence by assigning structural classes based on its location and environment and comparing the results to suitable structures.[31,51] Verify3D analysis revealed scores for TMEPAI isoform structure prediction using the trRosetta, RaptorX, Robetta, and AlphaFold servers of 2.62 to 79%, lower than the minimum criterion of >80%. The ERRAT scores of the TMEPAI isoform structure prediction ranged from 12 to 94%, and the score was lower than the minimum criterion of 91% for all predictions, excluding the TMEPAI-d prediction using trRosetta (91.13%) and TMEPAI-e prediction using Robetta (94.46%).[32] The QMEAN Z-scores for the TMEPAI isoform structure prediction from all servers ranged from −21.6 to 1.73. The high-quality prediction of the Z-score is close to 0, which means that the predicted structures are high-quality. QMEAN assesses the level of predicted structure authenticity compared to the exact size of experimental structures.[33] The QMEANBrane server assessment's c-score for the prediction quality must be 1, which means the structure is embedded in the membrane. The transmembrane domains of TMEPAI-a, TMEPAI-b, TMEPAI-d, and TMEPAI-e revealed that trRosetta server-based prediction exhibited a c-score of 1. Similarly, a c-score of 1 was recorded for TMEPAI-a, TMEPAI-b, and TMEPAI-e for RaptorX prediction. In contrast, all isoforms had a c-score of less than 1 for Robetta and AlphaFold server-based prediction. Meanwhile, TMEPAI-c had a c-score of <1 for all predictions. QMEANBrane determines the quality of the predicted transmembrane structure using statistical potentials targeted at the estimated local quality of membrane proteins at three different segments (membrane, interface, and soluble).[33]

The results of all validation assessments of the TMEPAI isoform structure predictions after comparing and analyzing each validation method (Table 4) illustrated that the trRosetta model was validated versus the other predictions. The QMEANBrane consideration assessment suggested that the structure is embedded in the membrane, and the TMHMM 2.0 parameter also provided a consistent result (Figure 4). The PROCHECK Ramachandran plot (most favored region) also confirmed that the prediction was validated, and 0% of residues were located in disallowed regions. The QMEAN and ERRAT values were consistent with these results. Validation analysis for TMEPAI isoforms suggested that the trRosetta model is the most reliable structure according to the QMEANBrane assessment and corresponding results using PROCHECK Ramachandran plots, Verify3D, QMEAN, and ERRAT. Because it can be considered that the model is structurally and stereochemically feasible and stable, the predicted structures of TMEPAI isoforms can be further used for protein function studies or simulations. The limitation of this study is that there is no crystal structure or experiment from the database (Protein Data Bank) that can be used as a comparison. The predicted structures of TMEPAI isoforms were consistent with previous findings indicating that TMEPAI localizes intracellularly, specifically within vesicles. Given that PY motif 1 (PPPY), PY motif 2 (PPTY), and SIM motif (PPNR) are exposed on the surface of the structure, they can



https://doi.org/10.1021/acsomega.4c08451
ACS Omega 2025, 10, 2712−2724

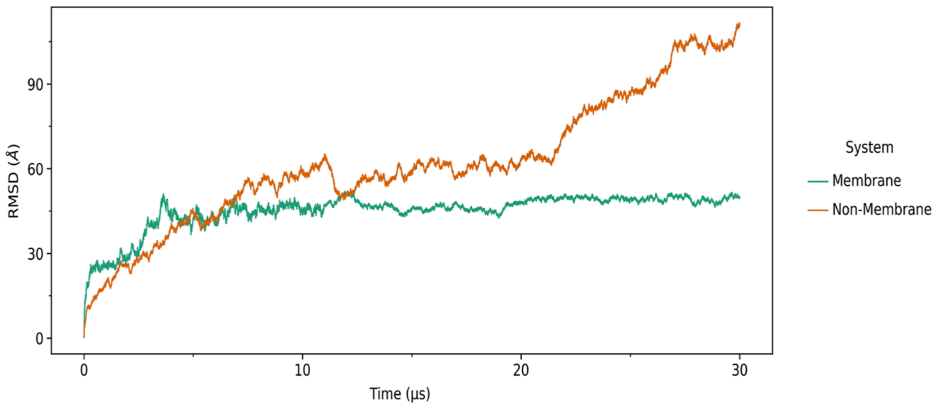


**Figure 6.** RMSD analysis comparison between membrane and nonmembrane systems.

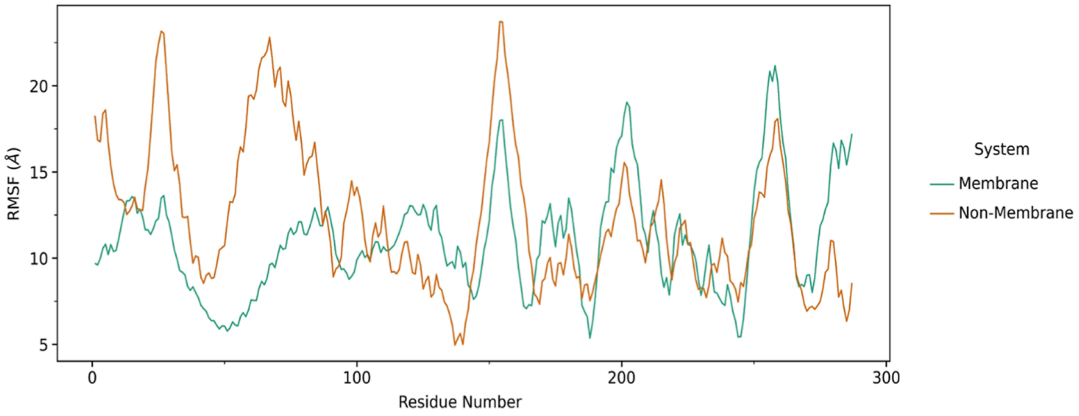


**Figure 7.** RMSF analysis comparison between membrane and nonmembrane systems.

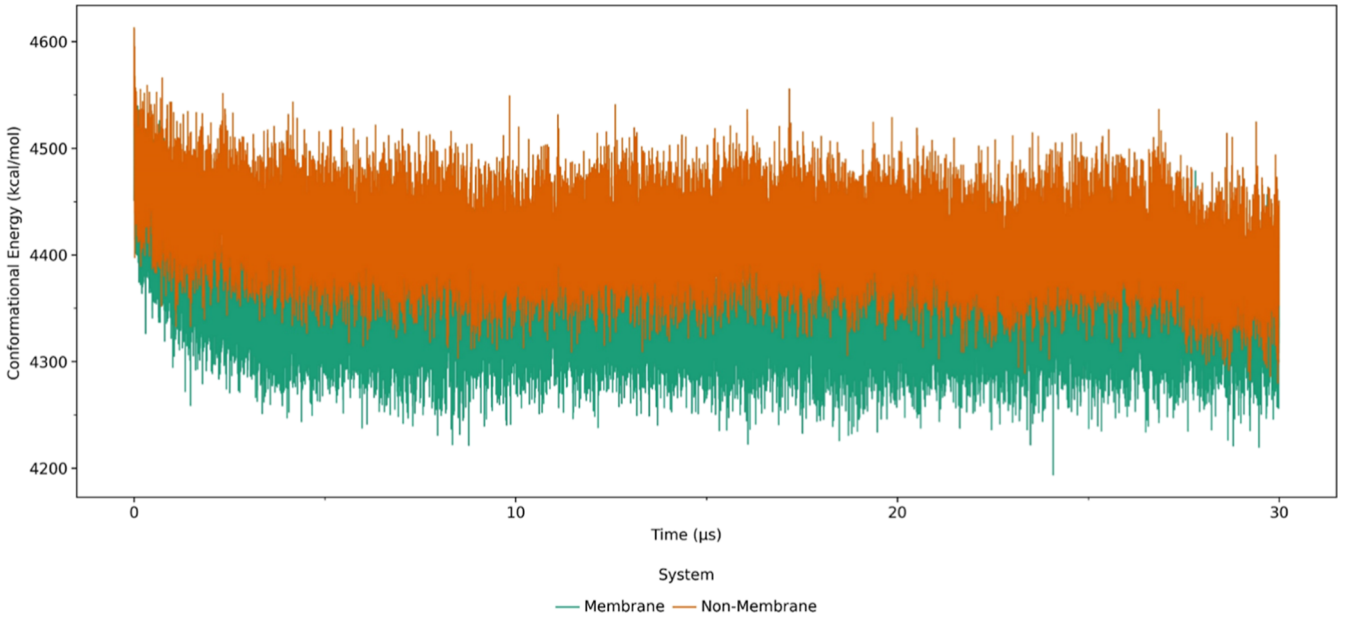


**Figure 8.** Conformational energy comparison between membrane and nonmembrane systems.

easily interact with TMEPAI-associated molecules or other solvents.

**CGMD Simulations of TMEPAI-A Protein and Trajectory.** TMEPAI-a simulated in CGMD during the structure refinement process requires the transmembrane system building to provide the right environment for transmembrane proteins to be integrated into the lipid bilayer membrane by embedding or embedding proteins in the lipid bilayer. Protein modeling has been refined using CGMD simulation through various methods that enable protein conformational changes, protein−protein interaction, protein−ligand binding, and protein-cell membrane interactions.[34,35] CGMD is especially



https://doi.org/10.1021/acsomega.4c08451
ACS Omega 2025, 10, 2712−2724

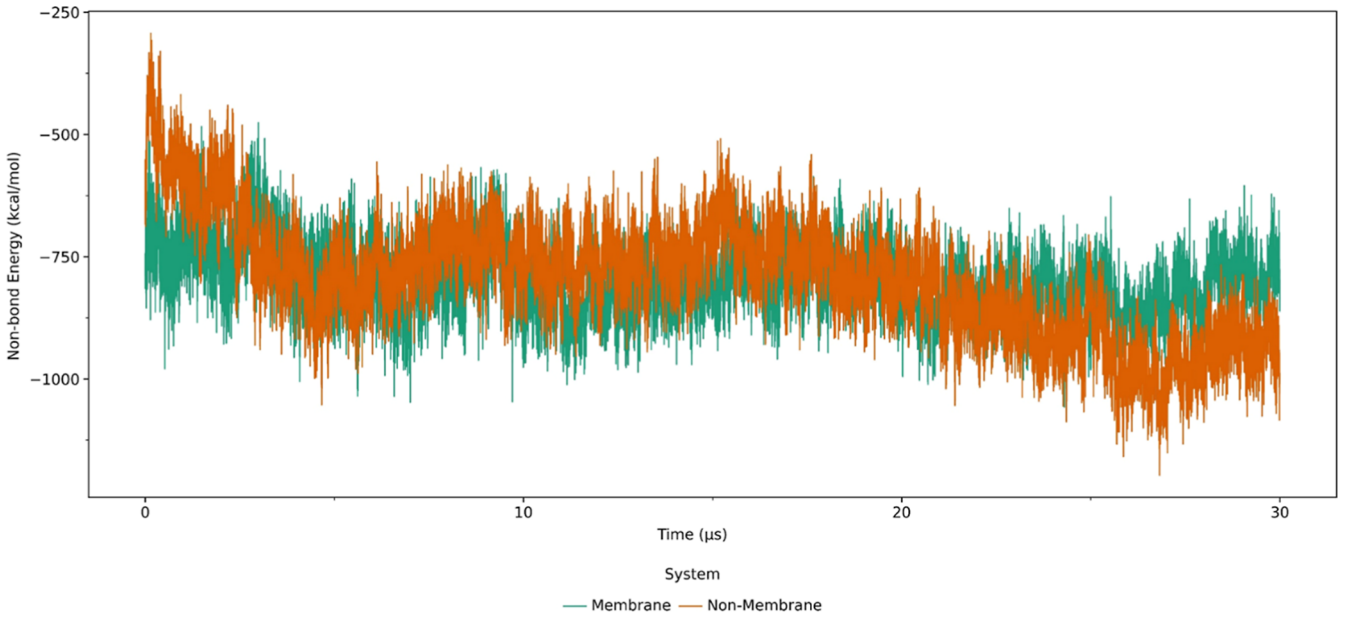


**Figure 9.** Nonbond energy comparison between membrane and nonmembrane systems.

advantageous, as it offers an appropriate approach for optimizing the three-dimensional structure of proteins within an environment that simulates the natural lipid bilayer. This approach allows for the efficient integration of TMEPAI into the membrane, considers protein−lipid interactions, and ensures that the protein assumes a conformation consistent with its biological role within the membrane.

The RMSD analysis of the TMEPAI-a CGMD simulation results with membrane and nonmembrane systems aims to compare the stability of conformational changes in the structure during the simulation process from the initial coordinate position between membrane and nonmembrane systems.[36] The graph of the RMSD analysis can be seen in Figure 6. The conformation of TMEPAI-a in the membrane system was more stable than that of the nonmembrane system during the simulation. The root-mean-square fluctuation (RMSF) analysis result of the TMEPAI-a in the membrane system during a 30 $\mu$s-length simulation (Figure 7) showed that conformational changes are not fluctuating in the protein residue transmembrane part in the TMEPAI-a structure compared to the nonmembrane system. Based on the results of the trajectory parameters in the CGMD simulation, it can be analyzed that TMEPAI-a in the membrane system has a more stable protein conformation, and the protein residue in the transmembrane part of TMEPAI-a did not fluctuate (residue numbers from 41 to 63, Figure 7) during the simulation when compared to TMEPAI-a in the nonmembrane system. This result is caused by the lipid bilayer membrane that affects the TMEPAI-a conformation and makes it more stable during the CGMD simulation.

The conformational energy of TMEPAI-a in the membrane system had lower energy compared to TMEPAI-a in the nonmembrane system, which means TMEPAI-a in the membrane system has a more stable conformation than the nonmembrane system and can be seen in Figure 8. The nonbond energy in the context of CGMD simulations is essential in protein binding affinity and conformational changes.[37] TMEPAI-a in the membrane system has a more stable nonbond energy than the nonmembrane system (Figure 9). The lipid bilayer membrane influences structural conformational refinement to become more stable in CGMD by affecting the environment of membrane proteins, lipid−protein interactions, and lipid diffusion.[38] The lipid bilayer membrane environment can affect the protein conformation stabilization compared to the nonmembrane system through its physical and chemical properties, distinct from the nonmembrane system.[39]

The uncertainty of atomic locations and thermal motion is measured by *B*-factors, which provide essential insights into the dynamics and flexibility of protein structures.[40,41] The transmembrane part in the TMEPAI-a in the membrane system showed low thermal motion or low *B*-factor, which indicates the structure is well ordered or stable (blue−green colors in Figure 10a) compared to the nonmembrane system having a high *B*-Factor or very flexible/fluctuates conformational changes (orange−red colors in Figure 10b).

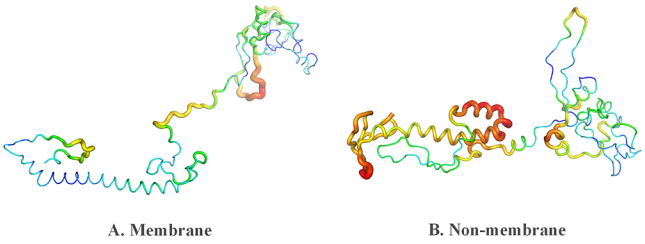


**Figure 10.** *B*-Factor analysis comparison between TMEPAI-a in the membrane and nonmembrane systems. (A) Membrane system and (B) nonmembrane system.

Trajectory similarity is the comparison of several molecular trajectories produced from CGMD simulations in terms of their structural and dynamic properties.[42] The results of trajectory similarity between TMEPAI-a in the membrane and nonmembrane systems showed no similarity. The visualization of TMEPAI-a in the membrane and nonmembrane systems is presented in Figures 11 and 12.

The closest protein homologue to TMEPAI is C18orf1, which shares a 61% sequence similarity. However, like



https://doi.org/10.1021/acsomega.4c08451
ACS Omega 2025, 10, 2712−2724

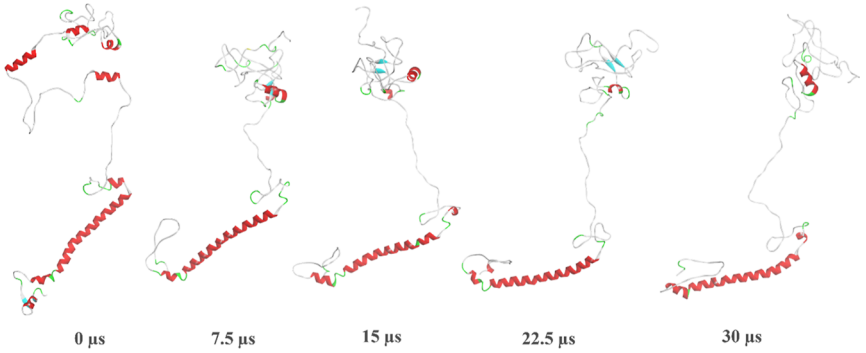


**Figure 11.** Visualization of TMEPAI-a in the membrane system.

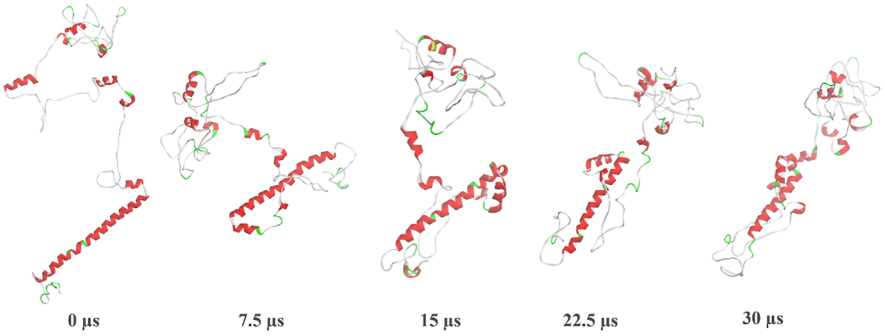


**Figure 12.** Visualization of TMEPAI-a in the nonmembrane system.

TMEPAI, C18orf1 does not have a crystal structure available. Additionally, no experimental structures in the Protein Data Bank can be used for comparison. The predicted structure is anticipated to provide a critical foundation for developing therapies targeting TMEPAI, but validation results showed that some methods are still deficient. However, it is imperative to emphasize that thorough exploration of computational methods and structural validation remains necessary to achieve a more reliable representation of the TMEPAI structure. Furthermore, crystallization of the TMEPAI protein is fundamental to elucidating its native structure and identifying specific interactions for the primary development of TMEPAI-targeting therapy.

## CONCLUSIONS

TMEPAI is well-known as a transmembrane protein that is highly expressed in breast cancer, colon cancer, and renal cell carcinoma tissues as well as in many other cancer cells. This protein was first identified as a prostatic protein induced by testosterone or its derivatives in the 2000 s. Many experiments suggest TMEPAI as a cancer drug target, but most TMEPAI research data are molecular and signaling mechanisms using in vitro and in vivo experiments without extensive structural experiments. Thereafter, the experimental data showed that TMEPAI is involved in multiple signaling and several signaling works paradoxically. So, inhibiting TMEPAI expression or diminishing TMEPAI action becomes impossible; many signals will be affected, and the off-target effect will increase. The essential idea is to predict the direct interaction of TMEPAI with specific proteins that involve carcinogenesis/tumorigenesis signaling and design the inhibitor or activator of these interactions. In this step, the TMEPAI structure is essential.

This study predicted the TMEPAI protein structure using the trRosetta, RaptorX, Robetta, and AlphaFold servers. Extensive evaluation was conducted to validate the prediction structure through the PROCHECK, QMEAN, QMEANBrane, Verify3D, and ERRAT servers. The trRosetta server emerged as the most reliable prediction structure. However, it is crucial to note that dynamic refinement steps are still needed to enhance the outcome. Computational protein structure prediction plays a central role in structure elucidation, as demonstrated in this study. The predicted structure is expected to provide the necessary foundation for the primary development of TMEPAI-targeting therapy. However, it is essential to emphasize that extensive exploration of computational methods and structural validation are still needed to obtain a more reliable TMEPAI structure. Furthermore, crystallization of the TMEPAI protein is also essential to elucidate its original structure and identify definite interactions.

## RESOURCES AVAILABILITY

**Lead Contact.** Assist data and requests for resources and reagents, which should be coordinated and will be satisfied by the lead contact, Riezki Amalia, email: riezki.amalia@unpad.ac.id.

**Materials Availability.** This study did not generate new unique reagents.

## EXPERIMENTAL MODEL AND SUBJECT DETAILS

This study did not include experimental models or subject details because it was computational research. Figure 1 shows the workflow for the TMEPAI structure prediction.

## METHOD DETAILS

**TMEPAI Isoforms Sequence and Alignment.** The FASTA format of the TMEPAI isoform sequences was



https://doi.org/10.1021/acsomega.4c08451
ACS Omega 2025, 10, 2712−2724

downloaded from NCBI (https://www.ncbi.nlm.nih.gov/). The accession numbers were as follows: TMEPAI-a, NP_064567; TMEPAI-b, NP_954638.1; TMEPAI-c, NP_954639.1; TMEPAI-d, NP_001242905.1; and ref Seq TMEPAI-e, ENST00000395819.3.20 The T-COFFEE Multiple Sequence Alignment Server (http://tcoffee.crg.cat/apps/tcoffee/do:tmcoffee) was used for TMEPAI isoform alignment.[43]

**TMEPAI Physicochemical Parameters and Secondary Structure Prediction.** ExPASy's ProtParam tool (https://web.expasy.org/protparam/) was used to determine the physicochemical parameters, namely, the theoretical isoelectric point, instability index, aliphatic index, and grand average of hydropathicity (GRAVY).[44] The PSIPRED server (http://bioinf.cs.ucl.ac.uk/psipred/) (Jones, 1999) was used to evaluate the secondary structure properties of TMEPAI isoforms. The RaptorX Property server (http://raptorx.uchicago.edu/StructurePropertyPred/predict/) and TMHMM 2.0 server (http://www.cbs.dtu.dk/services/TMHMM/) were used to predict the transmembrane helices in proteins.[45,46]

**Protein Modeling of TMEPAI Isoforms.** For TMEPAI structure prediction, the trRosetta,[29] RaptorX,[45] Robetta,[47] and AlphaFold[48] structure prediction servers were employed. The BIOVIA Discovery Studio Visualizer 2016 Client program was used to visualize the prediction result by opening the prediction structure in .pdb format.

**TMEPAI Protein Structure Prediction Validation.** PROCHECK suite programs, QMEAN SWISS-MODEL, QMEANBrane SWISS-MODEL, Verify3D, and ERRAT, were used to validate the predicted structures.[31−33,49−51] Figure 13 presents the research scheme displaying the analysis of physicochemical parameters, secondary structure predictions, and structure predictions using servers with different approaches and structure validation to assess the quality of the predicted structures.

**Transmembrane System Building.** The refined model was embedded into a POPC: POPE (3:2) membrane, resembling the major components of the human endoplasmic reticulum membrane,[52,53] using the PACKMOL-Memgen protocol.[54] Map the atomistic structure of the preassembled DMPC bilayer to its CG representation using amber_lipid.-map.[36]

**CGMD Simulations of TMEPAI Protein and Trajectory Analysis.** The Amber20 was used for the TMEPAI-a protein−bilayer membrane or nonmembrane systems in 3 $\mu$s-length simulations through several minimization steps to reach the lowest energy. The CGMD simulation of the TMEPAI protein in the bilayer membrane and the nonmembrane system was performed using the SIRAH 2.0 force field.[55] The heating process was performed in 3 stages of one-step heating from 0 K up to 310 K to resemble the human body temperature of about 37 °C. The equilibration processes were adapted according to the protocol of Ng et al., employing a time step of 2 fs.[56] The long-range electrostatics were treated using the particle mesh Ewald technique and the force field for proteins, lipids, water, and ions. The results of the CGMD simulation are visualized using visual MD to observe and analyze the interaction between the TMEPAI protein fold in the transmembrane and cytoplasm environments. The trajectories were analyzed by RMSD, RMSF, secondary structure protein analysis (DSSP analysis), protein volume, and principal component analysis in the *CPPTRAJ* program of Amber20.

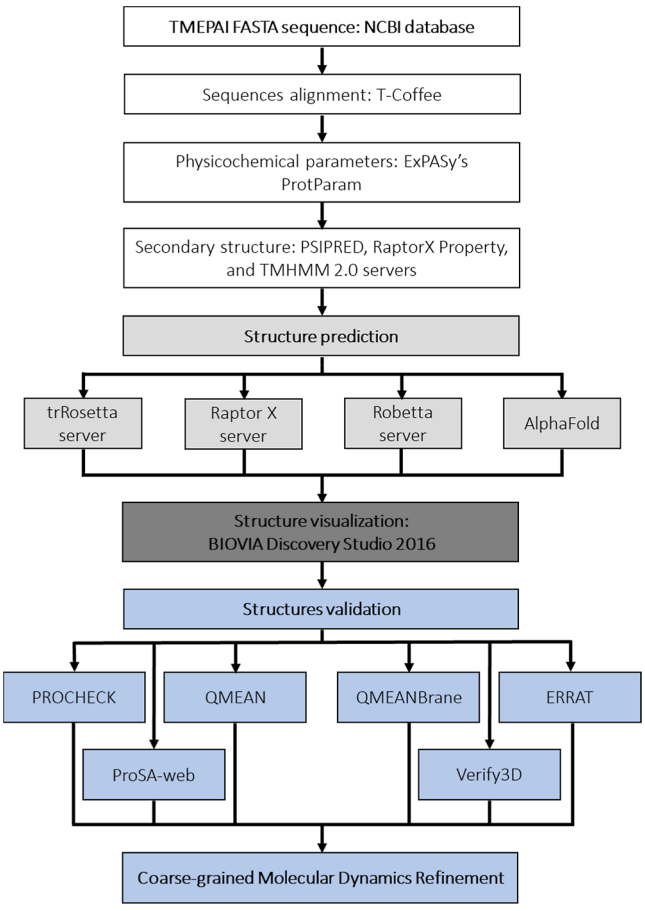


**Figure 13.** Workflow for TMEPAI structure prediction.

## ■ ASSOCIATED CONTENT

### Accession Codes

Accession no. (NCBI, https://www.ncbi.nlm.nih.gov/) of TMEPAI isoform-a NP_064567; TMEPAI isoform-b NP_954638.1; TMEPAI isoform-c NP_954639.1; TMEPAI isoform-d NP_001242905.1; and ref Seq TMEPAI isoform-e ENST00000395819.3.20

## ■ AUTHOR INFORMATION

### Corresponding Author

**Riezki Amalia** − *Department of Pharmacology and Clinical Pharmacy, Faculty of Pharmacy and Center of Excellence in Pharmaceutical Care Innovation, Universitas Padjadjaran, Bandung 45363, Indonesia; Laboratory of Translational Pharmaceutical Research, Faculty of Pharmacy, Universitas Padjadjaran, Bandung 45363, Indonesia;* orcid.org/0000-0002-8445-7045; Email: riezki.amalia@unpad.ac.id

### Authors

**Imam Adi Wicaksono** − *Department of Pharmacology and Clinical Pharmacy, Faculty of Pharmacy, Universitas Padjadjaran, Bandung 45363, Indonesia; Laboratory of Translational Pharmaceutical Research, Faculty of Pharmacy, Universitas Padjadjaran, Bandung 45363, Indonesia*

**Wanda Destiarani** − *Department of Chemistry, Faculty of Mathematics and Natural Sciences, Universitas Padjadjaran, Bandung 45363, Indonesia*



https://doi.org/10.1021/acsomega.4c08451
*ACS Omega* 2025, 10, 2712−2724

**Shidqi Fajri Romadhon** − *Department of Pharmacology and Clinical Pharmacy, Faculty of Pharmacy, Universitas Padjadjaran, Bandung 45363, Indonesia; Laboratory of Translational Pharmaceutical Research, Faculty of Pharmacy, Universitas Padjadjaran, Bandung 45363, Indonesia*

**Bagas Adi Prasetya Nugraha** − *Department of Pharmacology and Clinical Pharmacy, Faculty of Pharmacy, Universitas Padjadjaran, Bandung 45363, Indonesia; Laboratory of Translational Pharmaceutical Research, Faculty of Pharmacy, Universitas Padjadjaran, Bandung 45363, Indonesia*

**Muhammad Yusuf** − *Department of Chemistry, Faculty of Mathematics and Natural Sciences and Research Center for Molecular Biotechnology and Bioinformatics, Universitas Padjadjaran, Bandung 45363, Indonesia;* orcid.org/0000-0003-1627-1553

**Tiana Milanda** − *Department of Biology Pharmacy, Faculty of Pharmacy, Universitas Padjadjaran, Bandung 45363, Indonesia*

Complete contact information is available at: https://pubs.acs.org/10.1021/acsomega.4c08451

### Author Contributions

I.A.W. and R.A. conceptualized the study; I.A.W., W.D., S.F.R., and B.A.P.N. conducted the experiments; I.A.W., R.A., S.F.R., and B.A.P.N. analyzed the data; I.A.W. and R.A. wrote the manuscript, with contributions from T.M., W.D., and M.Y.; I.A.W., R.A., and T.M. acquired funding; T.M. and R.A supervised the project.

### Funding

The Grant from the Ministry of Education, Culture, Research and Technology, Republic of Indonesia, under the Doctoral Research Scheme 2023, contract no. 3018/UN6.3.1/PT.00/2023.

### Notes

The authors declare no competing financial interest.

## ■ ACKNOWLEDGMENTS

This work was supported by a Grant from the Ministry of Education, Culture, Research and Technology, Republic of Indonesia, under the Doctoral Research Scheme 2023 (for I.A.W., R.A., and T.M.).

## ■ REFERENCES

(1) Xu, L. L.; Shanmugam, N.; Segawa, T.; Sesterhenn, I. A.; McLeod, D. G.; Moul, J. W.; Srivastava, S. A novel androgen-regulated gene, PMEPA1, located on chromosome 20q13 exhibits high level expression in prostate. *Genomics* **2000**, *66* (3), 257−263.

(2) Giannini, G.; Ambrosini, M. I.; Di Marcotullio, L.; Cerignoli, F.; Zani, M.; MacKay, A. R.; Screpanti, I.; Frati, L.; Gulino, A. EGF and cell-cycle-regulated STAG1/PMEPA1/ERG1.2 belongs to a conserved gene family and is overexpressed and amplified in breast and ovarian cancer. *Mol. Carcinog.* **2003**, *38* (4), 188−200.

(3) Anazawa, Y.; Arakawa, H.; Nakagawa, H.; Nakamura, Y. Identification of STAG1 as a key mediator of a p53-dependent apoptotic pathway. *Oncogene* **2004**, *23* (46), 7621−7627.

(4) Nakano, N.; Itoh, S.; Watanabe, Y.; Maeyama, K.; Itoh, F.; Kato, M. Requirement of TCF7L2 for TGF-beta-dependent transcriptional activation of TMEPAI gene. *J. Biol. Chem.* **2010**, *285* (49), 38023−38033.

(5) Azami, S.; Vo Nguyen, T. T.; Watanabe, Y.; Kato, M. Cooperative induction of transmembrane prostate androgen induced protein TMEPAI/ PMEPA1 by transforming growth factor-$\beta$ and epidermal growth factor signaling. *Biochem. Biophys. Res. Commun.* **2015**, *456* (2), 580−585.

(6) Xu, L. L.; Shi, Y.; Petrovics, G.; Sun, C.; Makarem, M.; Zhang, W.; Sesterhenn, I. A.; McLeod, D. G.; Sun, L.; Moul, J. W.; Srivastava, S. PMEPA1, an androgen-regulated NEDD4-binding protein, exhibits cell growth inhibitory function and decreased expression during prostate cancer progression. *Cancer Res.* **2003**, *63*, 4299−4304.

(7) Li, H.; Xu, L. L.; Masuda, K.; Raymundo, E.; McLeod, D. G.; Dobi, A.; Srivastava, S. A feedback loop between the androgen receptor and a NEDD4-binding protein, PMEPA1, in prostate cancer cells. *J. Biol. Chem.* **2008**, *283* (43), 28988−28995.

(8) Watanabe, Y.; Itoh, S.; Goto, T.; Ohnishi, E.; Inamitsu, M.; Itoh, F.; Satoh, K.; Wiercinska, E.; Yang, W.; Shi, L.; Tanaka, A.; Nakano, N.; Mommaas, A. M.; Shibuya, H.; Ten Dijke, P.; Kato, M. TMEPAI, a transmembrane TGF-$\beta$-inducible protein, sequesters smad proteins from active participation in TGF-$\beta$ signaling. *Mol. Cell* **2010**, *37* (1), 123−134.

(9) Liu, R.; Zhou, Z.; Huang, J.; Chen, C. PMEPA1 promotes androgen receptor-negative prostate cell proliferation through suppressing the Smad3/4-c-Myc-p21Cip1 signaling pathway. *J. Pathol.* **2011**, *223* (5), 683−694.

(10) Amalia, R.; Abdelaziz, M.; Puteri, M. U.; Hwang, J.; Anwar, F.; Watanabe, Y.; Kato, M. TMEPAI/PMEPA1 inhibits Wnt signaling by regulating $\beta$-catenin stability and nuclear accumulation in triple negative breast cancer cells. *Cell. Signal.* **2019**, *59*, 24−33.

(11) Ji, J.; Ding, K.; Luo, T.; Xu, R.; Zhang, X.; Huang, B.; Chen, A.; Zhang, D.; Miletic, H.; Bjerkvig, R.; Thorsen, F.; Wang, J.; et al. PMEPA1 isoform a drives progression of glioblastoma by promoting protein degradation of the Hippo pathway kinase LATS1. *Oncogene* **2020**, *39* (5), 1125−1139.

(12) Li, Y.; Zhang, Y.; Li, L.; Zhang, M.; Song, N.; Zhao, Q.; Liu, Z.; Diao, A. TMEPAI promotes degradation of the NF-$\kappa$B signaling pathway inhibitory protein I$\kappa$B$\alpha$ and contributes to tumorigenesis. *Int. J. Biol. Macromol.* **2023**, *235*, 235123859.

(13) Tan, B.; Chen, Y.; Xia, L.; Yu, X.; Peng, Y.; Zhang, X.; Yang, Z. PMEPA1 facilitates non-small cell lung cancer progression via activating the JNK signaling pathway. *Cancer Biomarkers section A Dis Markers* **2021**, *31* (3), 203−210.

(14) Sharad, S.; Sztupinszki, Z. M.; Chen, Y.; Kuo, C.; Ravindranath, L.; Szallasi, Z.; Petrovics, G.; Sreenath, T. L.; Dobi, A.; Rosner, I. L.; Srinivasan, A.; Srivastava, S.; Cullen, J.; Li, H. Analysis of PMEPA1 isoforms (A and B) as selective inhibitors of androgen and Tgf-$\beta$ signaling reveals distinct biological and prognostic features in prostate cancer. *Cancers* **2019**, *11* (12), 1995.

(15) Haque, M. A.; Abdelaziz, M.; Puteri, M. U.; Vo Nguyen, T. T.; Kudo, K.; Watanabe, Y.; Kato, M. PMEPA1/TMEPAI Is a Unique Tumorigenic Activator of AKT Promoting Proteasomal Degradation of PHLPP1 in Triple-Negative Breast Cancer Cells. *Cancers* **2021**, *13* (19), 4934.

(16) Singha, P. K.; Pandeswara, S.; Geng, H.; Lan, R.; Venkatachalam, M. A.; Saikumar, P. TGF-$\beta$ induced TMEPAI/PMEPA1 inhibits canonical Smad signaling through R-Smad sequestration and promotes non-canonical PI3K/Akt signaling by reducing PTEN in triple negative breast cancer. *Genes Cancer* **2014**, *5* (9−10), 320−336.

(17) Rajkumar, T.; Vijayalakshmi, N.; Gopal, G.; Sabitha, K.; Shirley, S.; Raja, U. M.; Ramakrishnan, S. A. Identification and validation of genes involved in gastric tumorigenesis. *Cancer Cell Int.* **2010**, *10* (1), 45.

(18) Saadi, A.; Shannon, N. B.; Lao-Sirieix, P.; O'Donovan, M.; Walker, E.; Clemons, N. J.; Hardwick, J. S.; Zhang, C.; Das, M.; Save, V.; Novelli, M.; Balkwill, F.; Fitzgerald, R. C. Stromal genes discriminate preinvasive from invasive disease, predict outcome, and highlight inflammatory pathways in digestive cancers. *Proc. Natl. Acad. Sci. U.S.A.* **2010**, *107* (5), 2177−2182.

(19) Vo Nguyen, T. T.; Watanabe, Y.; Shiba, A.; Noguchi, M.; Itoh, S.; Kato, M. TMEPAI/PMEPA1 enhances tumorigenic activities in lung cancer cells. *Cancer Sci.* **2014**, *105* (3), 334−341.

(20) Sharad, S.; Dillman, A. A.; Sztupinszki, Z. M.; Szallasi, Z.; Rosner, I.; Cullen, J.; Srivastava, S.; Srinivasan, A.; Li, H. Characterization of unique PMEPA1 gene splice variants (isoforms d and e) from RNA Seq profiling provides novel insights into prognostic evaluation of prostate cancer. *Oncotarget* **2020**, *11* (4), 362−377.
(21) Rae, F. K.; Hooper, J. D.; Nicol, D. L.; Clements, J. A. Characterization of a novel gene, STAG1/ PMEPA1, upregulated in renal cell carcinoma and other solid tumors. *Mol. Carcinog.* **2001**, *32* (1), 44−53.
(22) Li, J.; Cao, R.; Cheng, J. A large-scale conformation sampling and evaluation server for protein tertiary structure prediction and its assessment in CASP11. *Bioinformatics* **2015**, *16* (1), 337.
(23) Zhu, S.; Liu, Y. Protein secondary structure online server predictive evaluation. *J. Phys. Conf. Series.* **2019**, *1237* (5), 052005.
(24) Patra, P.; Mondal, N.; Patra, B. C.; Bhattacharya, M. Epitope-based vaccine designing of Nocardia asteroides targeting the virulence factor Mce-family protein by immunoinformatics approach. *Int. J. Peptide Res. Ther* **2020**, *26* (2), 1165−1176.
(25) Lee, J.; Freddolino, P. L.; Zhang, Y. From Protein Structure to Function with Bioinformatics; In Rigden, D. J., Ed. 2nd edn.; Springer: Dordrecht, 2017; pp 3−35..
(26) Das, R.; Baker, D. Macromolecular modeling with rosetta. *Annu. Rev. Biochem.* **2008**, *77*, 363−382.
(27) Kelm, S.; Choi, Y.; Deane, C. M. Protein modeling and structural prediction. In *Springer Handbook of Bio-/Neuroinformatics*; 1st edn.; Kasabov, N., Ed.; Springer: Berlin, Heidelberg, 2014; pp 171−182..
(28) Hou, J.; Wu, T.; Cao, R.; Cheng, J. Protein tertiary structure modeling driven by deep learning and contact distance prediction in CASP13. *Proteins* **2019**, *87* (12), 1165−1178.
(29) Yang, J.; Anishchenko, I.; Park, H.; Peng, Z.; Ovchinnikov, S.; Baker, D. Improved protein structure prediction using predicted interresidue orientations. *Proc. Natl. Acad. Sci. U.S.A.* **2020**, *117* (3), 1496−1503.
(30) Ho, B. K.; Brasseur, R. The Ramachandran plots of glycine and pre-proline. *BMC Struct. Biol.* **2005**, *5* (14), 1−14.
(31) Bowie, J. U.; Luthy, R.; Eisenberg, D. A method to identify protein sequences that fold into a known three-dimensional structure. *Science* **1991**, *253* (5016), 164−170.
(32) Colovos, C.; Yeates, T. O. Verification of protein structures: patterns of nonbonded atomic interactions. *Protein Sci.* **1993**, *2* (9), 1511−1519.
(33) Studer, G.; Biasini, M.; Schwede, T. Assessing the local structural quality of transmembrane protein models using statistical potentials (QMEANBrane). *Bioinformatics* **2014**, *30* (17), i505−i511.
(34) Negami, T.; Shimizu, K.; Terada, T. Coarse-grained molecular dynamics simulation of protein conformational change coupled to ligand binding. *Chem. Phys. Lett.* **2020**, *742*, 137144−137146.
(35) Bradley, R.; Radhakrishnan, R. Coarse-Grained Models for Protein-Cell Membrane Interactions. *Polymers* **2013**, *5* (3), 890−936.
(36) Case, D. A.; Aktulga, H. M.; Belfon, K.; Cerutti, D. S.; Cisneros, G. A.; Cruzeiro, V. W. D.; Forouzesh, N.; Giese, T. J.; Götz, A. W.; Gohlke, H.; Izadi, S.; Kasavajhala, K.; Kaymak, M. C.; King, E.; Kurtzman, T.; Lee, T.-S.; Li, P.; Liu, J.; Luchko, T.; Luo, R.; Manathunga, M.; Machado, M. R.; Nguyen, H. M.; O'Hearn, K. A.; Onufriev, A. V.; Pan, F.; Pantano, S.; Qi, R.; Rahnamoun, A.; Risheh, A.; Schott-Verdugo, S.; Shajan, A.; Swails, J.; Wang, J.; Wei, H.; Wu, X.; Wu, Y.; Zhang, S.; Zhao, S.; Zhu, Q.; Cheatham, T. E., III; Roe, D. R.; Roitberg, A.; Simmerling, C.; York, D. M.; Nagan, M. C.; Merz, K. M., Jr; AmberTools, K. M. *J. Chem. Inf. Model.* **2023**, *63*, 6183−6191.
(37) Andrews, C. T.; Elcock, A. H. COFFDROP: A Coarse-Grained Nonbonded Force Field for Proteins Derived from All-Atom Explicit-Solvent Molecular Dynamics Simulations of Amino Acids. *J. Chem. Theory Comput.* **2014**, *10*, 5178−5194.
(38) Hall, B. A.; Chetwynd, A. P.; Sansom, M. S. P. Exploring Peptide-Membrane Interactions with Coarse-Grained MD Simulations. *Biophys. J.* **2011**, *100* (8), 1940−1948.
(39) Marx, D. C.; Fleming, K. G. Local Bilayer Hydrophobicity Modulates Membrane Protein Stability. *J. Am. Chem. Soc.* **2021**, *143* (2), 764−772.
(40) Li, D.-W.; Brüschweiler, R. All-Atom Contact Model for Understanding Protein Dynamics from Crystallographic B-Factors. *Biophys. J.* **2009**, *96* (8), 3074−3081.
(41) Kondrashov, D. A.; Cui, Q.; Phillips Jr, G. N. Optimization and Evaluation of a Coarse-Grained Model of Protein Motion Using X-Ray Crystal Data. *Biophys. J.* **2006**, *91* (8), 2760−2767.
(42) Kempfer, K.; Devemy, J.; Dequidt, A.; Couty, M.; Malfreyt, P. Development of Coarse-Grained Models for Polymers by Trajectory Matching. *ACS Omega* **2019**, *4*, 5955−5967.
(43) Chang, J. M.; Tomasso, P. D.; Taly, J. F.; Notredame, C. Accurate multiple sequence alignment of transmembrane proteins with PSI-Coffee. *BMC Bioinform* **2012**, *13* (Suppl4), S1.
(44) Gasteiger, E.; Hoogland, C.; Gattiker, A.; Duvaud, S.; Wilkins, M. R.; Appel, R. D.; Bairoch, A. Protein identification and analysis tools on the ExPASy server. In *The Proteomics Protocols Handbook*; Walker, J. M., Ed.; Springer Protocols Handbooks. Humana Press. 2005; pp 571−607. :571.
(45) Wang, S.; Li, W.; Liu, S.; Xu, J. RaptorX-Property: a web server for protein structure property prediction. *Nucleic Acid Res.* **2016**, *44*, 430−435.
(46) Krogh, A.; Larsson, B.; Von Heijne, G.; Sonnhammer, E. L. L. Predicting transmembrane protein topology with a hidden Markov model: Application to complete genomes. *J. Mol. Biol.* **2001**, *305* (3), 567−580.
(47) Kim, D. E.; Chivian, D.; Baker, D. Protein structure prediction and analysis using the Robetta server. *Nucleic Acids Res.* **2004**, *32*, 526−531.
(48) Jumper, J.; Evans, R.; Pritzel, A.; Green, T.; Figurnov, M.; Ronneberger, O.; Tunyasuvunakool, K.; Bates, R.; Žídek, A.; Potapenko, A.; Bridgland, A.; Meyer, C.; Kohl, S. A. A.; Ballard, A. J.; Cowie, A.; Romera-Paredes, B.; Nikolov, S.; Jain, R.; Adler, J.; Back, T.; Petersen, S.; Reiman, D.; Clancy, E.; Zielinski, M.; Steinegger, M.; Pacholska, M.; Berghammer, T.; Bodenstein, S.; Silver, D.; Vinyals, O.; Senior, A. W.; Kavukcuoglu, K.; Kohli, P.; Hassabis, D. Highly accurate protein structure prediction with AlphaFold. *Nature* **2021**, *596* (7873), 583−589.
(49) Laskowski, R. A.; MacArthur, M. W.; Moss, D. S.; Thornton, J. M. PROCHECK − a program to check the stereochemical quality of protein structures. *J. Appl. Cryst.* **1993**, *26*, 283−291.
(50) Benkert, P.; Biasini, M.; Schwede, T. Toward the estimation of the absolute quality of individual protein structure models. *Bioinformatics* **2011**, *27* (3), 343−350.
(51) Luthy, R.; Bowie, J. U.; Eisenberg, D. Assessment of protein models with three-dimensional profiles. *Nature* **1992**, *356* (6364), 83−85.
(52) Escribá, P. V.; Busquets, X.; Inokuchi, J.; Balogh, G.; Török, Z.; Horváth, I.; Harwood, J. L.; Vígh, L. Membrane lipid therapy: Modulation of the cell membrane composition and structure as a molecular base for drug discovery and new disease treatment. *Prog. Lipid Res.* **2015**, *59*, 38−53.
(53) Casares, D.; Escriba, P. V.; Rosello, C. A. Membrane Lipid Composition: Effect on Membrane and Organelle Structure, Function and Compartmentalization and Therapeutic Avenues. *Int. J. Mol. Sci.* **2019**, *20* (9), 2167−2196.
(54) Schott-Verdugo, S.; Gohlke, H. PACKMOL-Memgen: A Simple-To-Use, Generalized Workflow for Membrane-Protein−Lipid-Bilayer System Building. *J. Chem. Inf. Model.* **2019**, *59*, 2522−2528.
(55) Machado, M. R.; Barrera, E. E.; Klein, F.; Sonora, M.; Silva, S.; Pantano, S. The Sirah 2.0 Force Field: Altius, Fortius, Citius. *J. Chem. Theory Comput.* **2019**, *15* (4), 2719−2733.
(56) Ng, H. W.; Laughton, C. A.; Doughty, S. W. Molecular dynamics simulations of the adenosine A2 alfa receptor in POPC and POPE lipid bilayers: effects of membrane on protein behavior. *J. Chem. Inf. Model.* **2014**, *54*, 573−581.


https://doi.org/10.1021/acsomega.4c08451
*ACS Omega* 2025, 10, 2712−2724